Discrete element modeling of crack propagation in weak snowpack layers

Johan Gaume[1,*], Alec van Herwijnen[1], Jürg Schweizer[1], Guillaume Chambon[2] and Karl Birkeland[3]
[1] WSL Institute for Snow and Avalanche Research SLF, Davos, Switzerland
[2] IRSTEA, Grenoble, France
[3] USDA Forest Service National Avalanche Center, Bozeman, MT, USA

ABSTRACT: Dry-snow slab avalanches are generally caused by a sequence of fracture processes including (1) failure initiation in a weak snow layer underlying a cohesive slab, (2) crack propagation within the weak layer and (3) tensile fracture through the slab which leads to its detachment. During the past decades, theoretical and experimental work has gradually led to a better understanding of the fracture process in snow involving the collapse of the structure in the weak layer during fracture. This now allows us to better model failure initiation and the onset of crack propagation, i.e. to estimate the critical length required for crack propagation. On the other hand, our understanding of dynamic crack propagation is still very limited. For instance, it is not uncommon to perform field measurements with widespread crack propagation on one day, while a few days later, with very little changes to the snowpack, crack propagation does not occur anymore. Thus far, there is no clear theoretical framework to interpret such observations, and it is not clear how and which snowpack properties affect dynamic crack propagation. To shed more light on this issue, we performed numerical propagation saw test (PST) experiments applying the discrete element (DE) method and compared the numerical results with field measurements based on particle tracking. The goal is to investigate the influence of weak layer failure and the mechanical properties of the slab on crack propagation. Crack propagation velocities and distances before fracture arrest derived from the DE simulations were in good agreement with experimental data suggesting that the simulations can reproduce crack propagation in PSTs.

KEYWORDS: Snow avalanche, crack propagation, PST, discrete element modeling, slab, weak layer.

1 INTRODUCTION

Dry-snow slab avalanches result from the failure of a weak snow layer underlying cohesive slab layers. The local damage in the weak layer develops into a crack which can expand if its size exceeds a critical length or if the load exceeds a critical value. Finally, crack propagation leads to the tensile fracture of the slab and ultimately, avalanche release (McClung, 1979; Schweizer et al., 2003).

During the past decade our understanding of the fracture process in snow has gradually evolved through the development of new theories as well as various field observations and experiments. The propagation saw test (PST), concurrently developed by Gauthier and Jamieson (2006) and Sigrist and Schweizer (2007), allows one to determine the critical crack length and evaluate crack propagation propensity. This field method has highlighted the importance of slab bending (due to the collapsible nature of weak snow layers) on crack propagation (e.g. van Herwijnen et al., 2010). On the other hand, theoretical and numerical models, based on fracture mechanics or strength of material approaches, were developed to investigate crack propagation and avalanche release (McClung, 1979; Chiaia et al., 2008; Heierli, 2008; Gaume et al., 2013). While substantial progress has been made, application with regard to avalanche forecasting or hazard mapping is still hindered in part by our lack of understanding of the *dynamic* phase of crack propagation. For instance, it is not uncommon to perform PST field measurements with widespread crack propagation on one day, while a few days later, with seemingly very little changes in snowpack properties, cracks will no longer propagate. Thus far, there is no clear theoretical framework to interpret such observations, and it is not clear how and which snowpack properties affect dynamic crack propagation.

We performed numerical experiments of the propagation saw test (PST) applying the discrete element (DE) method and compared the numerical results with field measurements. The goal is to investigate the influence of weak layer failure and the mechanical properties of the slab on crack propagation. In a first section, the field data as well as the proposed model are pre-

Corresponding author address: Johan Gaume, WSL Institute for Snow and Avalanche Research SLF, Flüelastrasse 11, CH-7260 Davos Dorf, Switzrland;
tel: +33 6 748 23 547;
email: gaume@slf.ch

sented. Then, crack propagation speeds and distance before fracture arrest are derived from the DE simulations using the same method as for the field experiments (particle tracking). Finally, numerical and experimental results are compared and discussed.

2 DATA AND METHODS

2.1 PST field data

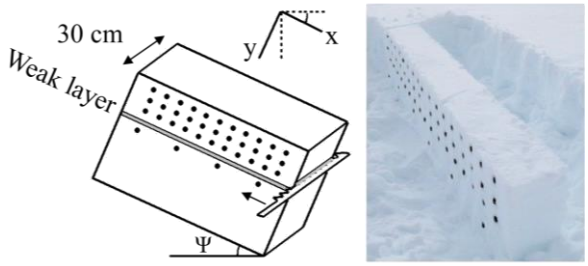

Fig. 1. Schematic drawing and picture of the propagation saw test (PST). The black dots are markers used for particle tracking in order to measure the displacement of the slab.

During the 2013-2014 winter, we collected data on seven separate days between 12 February and 1 April, by performing PST experiments on a layer of buried surface hoar at a study plot in southwestern Montana, USA (for more details see Birkeland et al., 2014). On each field day, we collected a manual snow profile and conducted one or several PSTs according to the procedure outlined in Greene et al., (2010). In many cases we used longer (than standard) beams to allow us to better investigate crack propagation. After PST preparation, we inserted black plastic markers into the pit wall and used a digital camera on a tripod to make a video recording of the PST (Fig. 1).

We used a particle tracking velocimetry (PTV) algorithm to analyze the motion of the markers and thus the displacement of the snow slab above the weak layer (Crocker and Grier, 1996). In this way, the position of the markers in each video frame can be determined with a mean accuracy of 0.1 mm. The displacement of a marker is then defined as the movement relative to its initial position, that is, the average position of the marker prior to movement. For propagating cracks, there is a delay between the vertical displacement of subsequent markers. The time delay between the onset of movement between markers is proportional to the distance between the markers and was used to calculate the propagation speed c of the fracture (van Herwijnen and Jamieson, 2005).

2.2 Discrete element model

2.2.1 Motivation and objectives

Discrete element (DE) modelling (Cundall and Stark, 1979) allows computing the motion of a large number of small particles by solving dynamic equations for each grain and assessing a contact law between the particles. Besides, the DE method allows assessing mechanical quantities such as stress, displacement, deformation rate, porosity, etc. at each material point within the sample. Experimentally, this would be an impossible task. Hence, using DE, the mechanical and rheological behaviour of the material can be explored locally, regardless of the spatial heterogeneities possibly displayed by the structure of the material and its mechanical quantities. This method can thus help to better understand physical processes at play in granular assemblies.

The DE method has been widely used to study the flow of granular materials within industrial (e.g. Chauduri et al., 2006; Sarkar et al., 2010) or environmental applications such as snow dynamics (e.g. Rognon et al., 2008; Faug et al., 2009). However, to our knowledge, discrete elements have never been used to model crack propagation in layered systems or to describe slab avalanche release processes. The latter processes are generally modelled under a continuum mechanics framework, using methods such as finite elements (Podolskiy et al., 2013 and references therein). While these methods can be used to assess the stability of a layered snow cover, i.e. determine the conditions of failure occurrence and the onset of crack propagation, they are not suited to study what occurs after failure, i.e. the dynamic phase of crack propagation.

The objective of the proposed approach is to use the DE method to model the structure of both the slab and the WL using discrete cohesive particles. This will allow mimicking the high porosity of the WL and to account for slab elasticity and for the different modes of failure possibly displayed by snow (shear, compression, tension). Ultimately, DE propagation saw tests will be performed to investigate the characteristics of crack propagation.

2.2.2 Formulation of the model

The discrete element simulations were performed using the commercial software PFC2D (by Itasca), which implements the original soft-contact algorithm described in Cundall and Strack (1979). The simulated system is two dimensional and is composed of a completely rigid basal layer, a WL of thickness h_{wl} = 4.5 cm and a slab of thickness h = 20 cm. The slab is composed of grains of radius r = 0.01 m with a primitive cubic packing (or isometric). The porosity of the slab is equal to 21%. Hence the

density of the slab ρ can be adjusted by changing the particle density ρ_p (varied in the simulations). The WL is composed of grains of radius $r_{wl} = r/2$ with a complex packing of collapsible triangular forms aimed at roughly representing the porous structure of persistent WLs such as surface hoar or depth hoar. The porosity of the WL is 70% and the density of the WL grains is $\rho_{wl} = 400$ kg/m^3. The length of the system is $L = 2$ m and in a first step, the simulations were performed for a slope angle equal to zero (which is not always the case in the experiments). Concerning the system dimensions, a relatively high thickness was chosen for the WL in order to clearly observe bending effects and the collapse. On the other hand, the grain sizes were chosen relatively large and the slab relatively thin so as to reduce the computational time. It is also worth noting that the numerical grains are not indented to represent the real snow grains which are obviously smaller. Nevertheless, as will be shown, this set up allows us to capture the main features observed in field PSTs.

The loading is applied by gravity and translation of a "saw" (in red on Fig. 3) at a constant velocity $v_{saw} = 2$ m/s. This saw is composed by rigid walls and has approximately the same thickness as field saws $h_{saw} = 2$ mm. The saw velocity was chosen relatively high to decrease the computational time but also to be lower than the lowest crack propagation speed observed in the field so as to correctly distinguish crack propagation from the saw movement.

A classical interparticle contact law was used in the simulations (Radjai and Dubois, 2011). The normal force is the sum of a linear elastic and of a viscous contribution (spring-dashpot model), and the tangential force is linear elastic with a Coulombian friction threshold. The corresponding mechanical parameters, namely the normal and shear stiffness k_n and k_s (elasticity parameters), the restitution coefficient (viscous parameter) and the friction coefficient μ are summarized in Tab. 1. The value of the normal stiffness k_n was chosen in such a way that the normal interpenetrations at contacts is kept small, i.e. to work in the quasi-rigid grain limit (Da Cruz et al., 2005; Roux and Combe, 2002). Concerning the normal restitution coefficient e, we checked that the results presented below, and more generally all the macroscopic mechanical quantities obtained from the simulations, are actually independent of this parameter (in the range 0.1 - 0.9), in agreement with previous studies (Da Cruz et al., 2005; Gaume et al., 2011).

Cohesion was added to the particles by adding a bond at each contact. A contact bond can be envisioned as a point of glue with constant normal and shear stiffness k_n^b and k_s^b acting at the contact point (Fig. 2). This bond has a specified shear and tensile strength σ_t and σ_s. If the magnitude of the tensile stress exceeds the bond tensile strength, the bond breaks and both the normal and shear contact forces are set to zero. If the magnitude of the shear stress exceeds the bond shear strength, the bond also breaks but the contact forces are not altered, provided that the shear force does not exceed the friction limit, and provided that the normal force is compressive. The ranges of parameters used for the bond model are summarized in Tab. 2.

Tab. 1. Mechanical parameters used in the simulations for the contact law. k_n: normal contact stiffness; k_s: tangential contact stiffness; μ: intergranular friction; e: normal restitution coefficient.

k_n (N/m)	k_n/k_s	μ	e
1.10^4	2	0.5	0.1

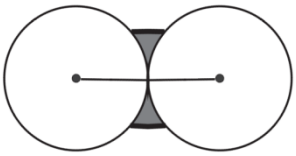

Fig. 2. Scheme of the cohesive bond used in the simulations.

Tab. 2. Mechanical parameters used in the simulations for the cohesive law. k_n^b: bond normal stiffness; k_s^b: bond shear stiffness; σ_t : bond tensile strength; σ_s : bond shear strength.

	k_n^b (Pa/m)	k_n^b/k_s^b	σ_t (Pa)	σ_t/σ_s
slab	10^7-10^{10}	2	10^3 - 2×10^4	2
WL	1×10^{10}	2	1.6×10^4	2

2.2.3 Simulation protocol

First, before performing the PST simulations, the slab Young's modulus must be determined as a function of the microscopic properties of the bond. Hence, biaxial tests were carried out and allowed to determine the macroscopic Young's modulus of the slab as a function of the bond stiffness. Similarly, simple loading tests were carried out to compute the macroscopic failure criterion (mixed mode shear-compression) of the WL as a function of the bonds of WL grains.

Then, in order to determine the crack propagation speed, purely elastic simulations (infinite tensile and shear strength) were performed for different slab densities with a Young's modulus

varying according to an empirical exponential fit to the data reported by Scapozza (2004):

$$E = 1.873 \times 10^5 \, e^{0.0149\rho} \qquad (1)$$

The crack propagation speed was obtained from the evolution of slab displacement over time using the same algorithm as that used by van Herwijnen and Jamieson (2005) for field tests. The only difference is that with DE we do not need markers since we have access to the displacement of every particle of the system.
Finally, to compute the propagation distance, the possible failure of the slab was taken into account by introducing a realistic tensile strength, function of slab density, according to a power-law fit of the data reported by Sigrist, (2006) using the three point bending fracture test:

$$\sigma_t = 2.4 \times 10^5 \left(\frac{\rho}{\rho_{ice}}\right)^{2.44} \qquad (2)$$

with $\rho_{ice} = 917$ kg/m^3.

3 RESULTS

Simulations were performed for slab densities ranging from 100 to 300 kg/m^3, corresponding to a Young's modulus E of the slab between 0.8 and 16 MPa. An example is given in Fig. 3 for a density of 100 kg/m^3, where one can clearly see slab bending prior to the onset of crack propagation (for a critical length of 20 cm) and the dynamic propagation phase. These distinct phases are also clearly visible in the vertical displacement Δy, as shown in Fig. 4 for four different horizontal positions in the slab.

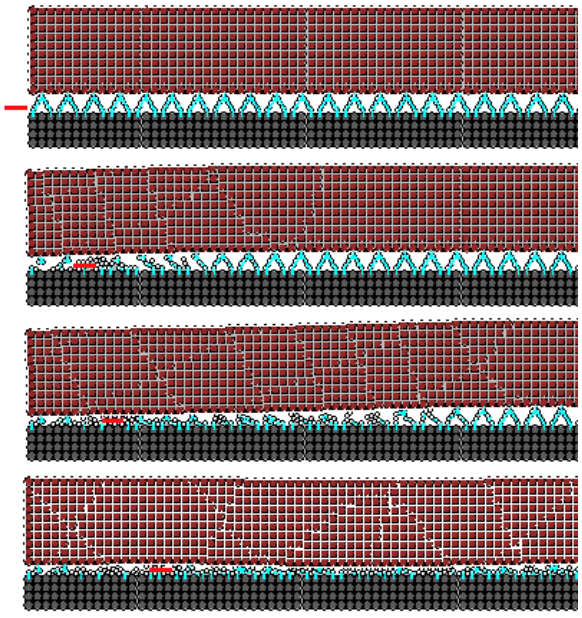

Fig. 3. Snapshots of a PST numerical experiment. (a) Initial system t = 0.1 s, (b) onset of crack propagation t = 0.26 s, (c) dynamic propagation t = 0.28 s; (d) complete failure of the WL t = 0.45 s.

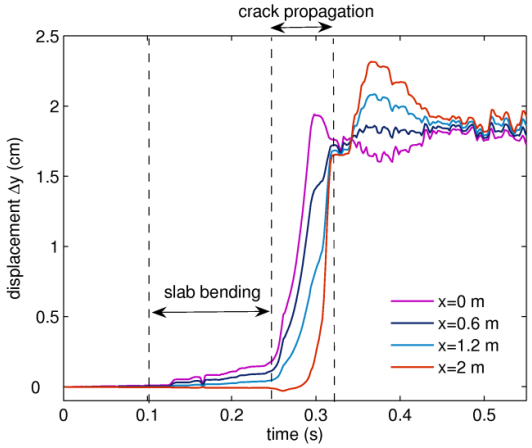

Fig. 4. Temporal evolution of the modeled vertical displacement Δy of the slab for a slab density ρ = 250 kg/m^3. The different curves correspond to different horizontal positions of the slab, from the left-end (x = 0 m) to the right-end (x = 2 m).

Between 0 and 0.1 s nothing happens, then as the saw advances, the vertical displacement slowly increases. This phase corresponds to the bending of the slab on the left side of the saw. Then, for t = 0.25 s approximately, the displacement increases abruptly, even beyond the saw, corresponding to the dynamic crack propagation phase. After t = 0.3 s, the slab has reached the broken WL at the left-end of the slab for x = 0 m. After 0.32 s, the entire WL has collapsed leading to a constant vertical displacement of the slab approximately equal to Δy = 1.8 cm. This displacement is not perfectly equal to the WL thickness because of the particles remaining in the WL. The peak in the displacement around t = 0.38 s corresponds to the translation of the saw after the crack has propagated.

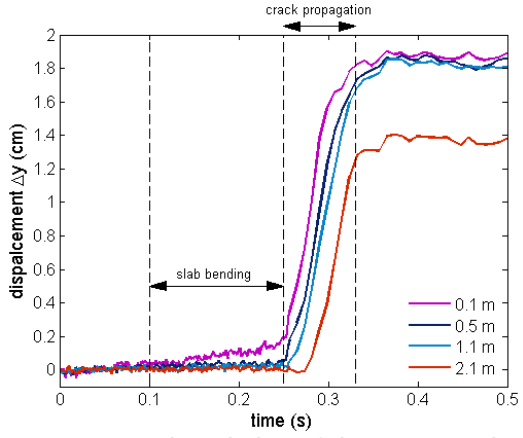

Fig. 5: Temporal evolution of the measured vertical displacement Δy for a slab density of ρ = 240 kg/m^3. The different curves correspond to different horizontal positions of the slab, from the left-end (x = 0 m) to the right-end (x = 2 m).

These numerical results are in good agreement with experimental results (Fig. 5). Indeed, the same phases in the displacement curves, corresponding to slab bending and crack propagation, are observed in the measurements. Furthermore, the amount of slope normal displacement prior to crack propagation as well as the fracture time, defined as the time it takes for the slab to come into contact with the broken weak layer, were very similar. Finally, we would like to point out that the total slope normal displacement after crack propagation in our experimental results was not constant for all markers, which is consistently observed in field experiments (e.g. van Herwijnen et al., 2010; Bair et al., 2014), whereas it is approximately constant in the numerical simulations.

3.1 Crack propagation speed

As explained before, for both numerical and field experiments, the crack propagation speed was determined from the slab displacement using the algorithm described in van Herwijnen and Jamieson (2005). In the field experiments, slab displacement was obtained through particle tracking velocimetry (PTV) using black markers on the sample (Fig. 1). The crack propagation speed *c* obtained in field PSTs and from the simulated PSTs is represented as a function of slab density. Overall, the propagation speed obtained from field PSTs increased from 10 to 50 m/s as the density increased from 140 to 280 kg/m^3 (Fig. 6). The blue squares represent the cases with fracture arrest due to tensile fracture of the slab for which the crack propagation speed is not very accurate and generally lower than the velocity measured when the slab did not break. Overall, the model reproduces the increasing trend with slab density well. Whereas the simulations were performed for a constant slab depth, the slab depth generally increased with increasing density in the field experiments. Speed values from the simulations would be higher for high densities if the increase of slab depth was also taken into account. Indeed, we performed some simulations in which only one parameter was varied which showed that crack propagation velocity increases with increasing slab density, Young's modulus, slab depth and WL thickness. The latter result is not compatible with the expression for crack propagation speed proposed by Heierli (2008) for which the velocity decreases with increasing WL thickness.

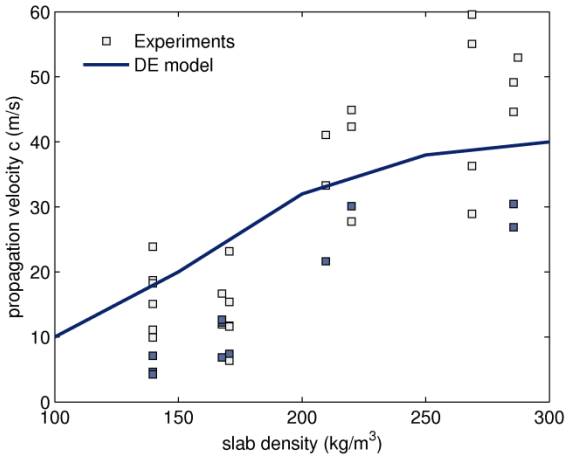

Fig. 6. Crack propagation speed vs slab density. The squares correspond to field PST and the filled squares correspond to PST with fracture arrest. The continuous line corresponds to the result of the DE model taking into account the link between slab density and Young's modulus for a slab depth h = 20 cm and a zero slope angle.

3.2 Propagation distance

To determine the propagation distance, Eq. (2) was used to compute the tensile strength σ_t. The simulated range of densities thus corresponds to values of tensile strength varying between 1 and 15 kPa. Fig. 7 shows that overall the propagation distance obtained from field experiments increased with increasing density. This trend is very well reproduced by the discrete element simulations. We recall that the simulations were performed only for a zero slope angle and thus tensile stresses in the slab are only due to bending. Of course, the propagation distance is limited by the length of the beam which was equal to 2 m in the simulations and which ranges between 1 and 2.6 m in the experiments. These results confirm that dense and hard snow slabs are more prone to widespread crack propagation than soft slabs. Besides, one can assume that above a certain density, the maximum tensile stress in the slab no longer exceeds the tensile strength. Indeed, during crack propagation the slab comes in contact with the broken WL, which limits the increase of the tensile stress with density, whereas the tensile strength still increases with density according to Eq. 2. Hence, for high densities, we expect that the mechanical properties of the snowpack only marginally affect crack propagation distance in the field, but that terrain characteristics and snowpack spatial variability play a crucial role.

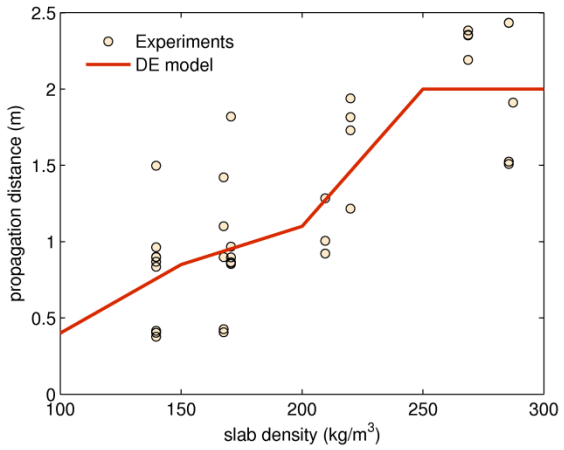

Fig. 7. Propagation distance vs slab density. The circles correspond to field PSTs. The continuous line corresponds to the result of the DE model taking into account the link between slab density, Young's modulus and tensile strength for a slab depth h = 20 cm and a zero slope angle.

4 DISCUSSION AND CONCLUSIONS

We proposed a new approach to characterize crack propagation in weak snowpack layers using the discrete element method with elastic-brittle bonded grains. This model allowed us to precisely compute crack propagation velocity from slab vertical displacement as a function of snowpack properties. Modelled velocities were in good agreement with those obtained from field measurements.

Furthermore, crack propagation distance was computed by implementing the tensile strength of the slab obtained from laboratory tests (Sigrist, 2008). Again, numerical results well reproduced the trend observed in the field experiments. In particular, the propagation distance was found to increase from approx. 0.5 m to 2 m, the beam length, when slab density increased from 100 to 250 kg/m^3. This is a very interesting result, since the propagation distance l_0 required to regain contact between the unsupported bending slab and the broken WL is typically lower than 2 m, for realistic values of the snowpack parameters (this length can be easily computed from the classical beam theory, Timoshenko and Goodier, 1970). While the maximum tensile stress in the slab increases with crack length, it will reach a constant value as soon as the unsupported slab touches the WL. On the other hand, the tensile strength increases with slab density (Eq. 2), so that for a given density value, the tensile strength will be higher than the tensile stress, leading to the absence of tensile fracture through the slab and thus wide-spread crack propagation. According to our simulation and field measurements, this critical density is between 200 and 250 kg/m^3. For slabs denser than this value, the slab tensile fracture in the field may be controlled by topographical and morphological features of the path such as rocks, trees, terrain breaks, etc. but also by the spatial heterogeneity of the snow cover. This result also suggests that the beam length of propagation saw tests should not be lower than 2 m, in agreement with the recent study of Bair et al. (2014) about PST edge effects.

More DE simulations will be carried out for different slope angles, slab depths and WL properties in order to find a widely applicable model for the propagation speed and distance as a function of dimensionless parameters of the system. Finally, different and more complex structures for the WL will also be implemented with the long-term objective of modelling the structure of the WL directly from segmented micro-tomographic images (Hagenmuller et al., 2014).

5 REFERENCES

Bair, E. H., Simenhois, R., van Herwijnen, A., and Birkeland, K. (2014). The influence of edge effects on crack propagation in snow stability tests. *The Cryosphere Discussions*, *8*(1), 229-257.

Birkeland, K., van Herwijnen, A., Staples, M., Knoff, E., Bair, E., Simenhois, R., (2014). The role of slabs and weak layers in fracture arrest. Proceedings of the ISSW 2014. Banff – Canada.

Chaudhuri, B., A. Mehrotra, F. J. Muzzio, and M. S. Tomassone (2006), Cohesive effects in powder mixing in a tumbling blender, Powder Technol., 165(2), 105–114.

Chiaia, B., P. Cornetti, and B. Frigo (2008), Triggering of dry snow slab avalanches: stress versus fracture mechanical approach, Cold Reg. Sci. Technol., 53, 170-178.

Cundall, P. A., and O. D. Strack (1979), A discrete numerical model for granular assemblies, Geotechnique, 29(1), 47–65

Crocker, J.C., D.G. Grier, 1996. Methods of digital video microscopy for colloidal studies. Journal of Colloid Interface Science, 179 (1), 298-310.

Greene, E. M., et al. (2010), Snow, Weather and Avalanches: Observation guidelines for avalanche programs in the United States, 2nd ed., 150 pp., American Avalanche Association, Pagosa Springs, Colorado.

Faug, T., R. Beguin, and B. Chanut (2009), Mean steady granular force on a wall overflowed by free-surface gravity-driven dense flows, Phys. Rev. E, 80(2), 021305.

Gaume, J., G. Chambon, N. Eckert, and M. Naaim (2013), Inuence of weak-layer heterogeneity on snow slab avalanche release: Application to the evaluation of avalanche release depths., J. Glaciol., 59(215), 423-437.

Gauthier, D., and B. Jamieson, Evaluation of a prototype field test for fracture and failure

propagation propensity in weak snowpack layers, Cold Reg. Sci. Technol., 51 (2), 87-97.

Hagenmuller, P., Chambon, G., Lesaffre, B., Flin, F., & Naaim, M. (2013). Energy-based binary segmentation of snow microtomographic images. *J. Glaciol.*, *59*(217), 859-873.

Heierli, J., (2008), Anticrack model for slab Avalanche release, PhD thesis, Karlsruhe University.

van Herwijnen, A., and J. B. Jamieson (2005), High speed photography of fractures in weak layers, Cold Reg. Sci. Technol., 43(1-2), 71-82.

van Herwijnen, A., Schweizer, J., Heierli, J. (2010). Measurement of the deformation field associated with fracture propagation in weak snowpack layers. *J. Geophys. Res., 115, F03042.*

McClung, D. (1979), Shear fracture precipitated by strain softening as a mechanism of dry slab avalanche release, J. Geophys. Res., 84(B7), 3519-3526.

Podolskiy, E. A., Chambon, G., Naaim, M., and Gaume, J. (2013). A review of finite-element modelling in snow mechanics. J. Glaciol.,59(218), 1189-1201.

Rognon, P., J.-N. Roux, M. Naaim, and F. Chevoir (2008), Dense flows of cohesive granular materials, J. Fluid Mech., 596, 21-47.

Roux, J. N., & Combe, G. (2002). Quasistatic rheology and the origins of strain.Comptes Rendus Physique, 3(2), 131-140.

Sarkar, A., and C.Wassgren (2010), Continuous blending of cohesive granular material, Chemical Engineering Science, 65(21), 5687-5698.

Scapozza, C. (2004), Entwicklung eines dichte- und temperaturabhängigen Stoffgesetzes zur Beschreibung des viskoelastischen Verhaltens von Schnee, Ph.D. thesis, ETH Zurich.

Schweizer, J., B. Jamieson, and M. Schneebeli (2003), Snow avalanche formation, Rev. Geophys., 41(4), 1016.

Sigrist, C., and J. Schweizer (2007), Critical energy release rates of weak snowpack layers determined in field experiments, Geophys. Res. Lett., 34 (3), L03502.

Sigrist, C. (2006), Measurements of fracture mechanical properties of snow and application to dry snow slab avalanche release, Ph.D. thesis, ETH Zurich.

Timoshenko, S.P. and J.N. Goodier (1970). Theory of Elasticity. McGraw-Hill, 608 pp.